Supporting Information

Enhancement of Hybrid Organohydrogels by Interpenetrating Crosslinking Strategies for Multi-Source Signal Recognition over a Wide Temperature Range

Shen Zhang, Rui Sun, Jun Wang, Zhiqin Jiang, Mingfang Liu, Hua Chen, Zhijun Hu, Xiaoli Zhan, Feng Gao, Qinghua Zhang**

S. Zhang, R. Sun, J. Wang, Z. Jiang, Dr. F. Gao, X. Zhan and Prof. Q. Zhang

Zhejiang Provincial Key Laboratory of Advanced Chemical Engineering Manufacture Technology, College of Chemical and Biochemical Engineering, Zhejiang University, Hangzhou, 310027, China.

Dr. F. Gao, X. Zhan and Prof. Q. Zhang

Institute of Zhejiang University-Quzhou, Zhejiang Provincial Innovation Center of Advanced Chemicals Technology, Quzhou 324000, China.

X. Zhan and Prof. Q. Zhang

Donghai Laboratory of Zhejiang University, Zhoushan, 316000, China.

M. Liu, H. Chen and Prof. Z. Hu

Zhejiang University of Science and Technology, School of Environment and Natural Resources, Hangzhou 310023, China

*Corresponding author E-mail: feng_gao@zju.edu.cn; qhzhang@zju.edu.cn

Supporting information mainly contains the following contents:

4. Supplementary References

1. Supplementary Methods

Materials: Acrylamide (AM, 99%), Sodium dodecyl sulfate (SDS, 99%), N, N'-Methylenebis (2-propenamide) (MBAA, 99%), Carboxymethylcellulose sodium (CMC), Glycerol(99%), Octadecyl Methacrylate(C_{18},96%), $CaCl_2 \cdot 2H_2O$(99%), Ammonium persulphate(APS,98%) and Tannic acid (TA, 95%) were purchased from Shanghai Aladdin Biochemical Technology Co., Ltd. Polyethylenimine branched (PEI, M_w 10000, 98%) was bought from Beijing Hwrk Chemical Co., Ltd. Deionized water was used for all the experiments.

Preparation of AC hydrogel:

AM (2.84 g, 39.95 mmol), MBAA (0.0032 g, 0.02 mmol), and APS (0.46 g, 1.98 mmol) were typically dissolved in DI water (20 ml) with stirring at room temperature for 5 min. After that, $CaCl_2 \cdot 2H_2O$ (0.22 g, 1.50 mmol) and CMC (0.30 g, 1.24 mmol) were added to obtain an AC precursor solution, poured the precursor solution into the mold to initiate polymerization by exposing it to UV light for 30 minutes to obtain AC hydrogel.

Preparation of ACC hydrogel:

SDS (0.27 g, 0.93 mmol) and glycerol (10 ml) were typically dissolved in DI water (10 ml) with stirring at 50 ^oC for 1 h. After that, C_{18} (0.17 g, 0.52 mmol) was added. Following sonication for 3 min in ice water (2 s working time, 3 s pulse mode, 350 W), AM (2.84 g, 39.95 mmol) and MBAA (0.0032 g, 0.02 mmol) were added and stirred for 5 min at room temperature, and then added $CaCl_2 \cdot 2H_2O$ (0.22 g, 1.50 mmol), CMC (0.30 g, 1.24 mmol), and APS (0.46 g, 1.98 mmol) to obtain ACC precursor solution, poured the precursor solution into the mold to initiate polymerization by exposing to UV light for 30 minutes to obtain ACC hydrogel.

Preparation of PEI-TA bionic binder: PEI and TA were typically dissolved in DI water at 40 mg mL^{-1}, respectively. Following that, 10 mL PEI solution and 10 mL TA solution were mixed at 25 ^{o}C, and added 0.1 M HCl solution to the mixture to adjust the pH to 4.2.

Preparation of ACC-PT organohydrogel:

First, the ACC precursor solution and PEI-TA bionic binder were prepared as previously described. Subsequently, 2 g of PEI-TA bionic binder was added to the ACC precursor solution and stirred for 30 minutes at room temperature to obtain the ACC-PT precursor solution, poured the precursor solution into the mold to initiate polymerization by exposing it to UV light for 30 minutes to obtain ACC-PT organohydrogel.

Statement: The participants for the real-life test for organohydrogel-based sensors were the authors (S.Z and R.S) of this article, who took part following informed consent and have provided informed consent. Ethical approval was not required for this work.

Characterization: The chemical structure of AC, ACC, ACC-PT, and PEI-TA was measured by Fourier transform infrared spectroscopy (FTIR, Nicolet5700 spectrometer). A scanning electron microscope (SEM, Phenom XL) was used to observe the morphologies and microstructures of ACC-PT organohydrogel after lyophilization. An X-ray photoelectron spectrometer (XPS, Thermo Scientific K-Alpha) was used to analyze the surface elemental composition of AC, ACC, and ACC-PT.

Adhesive Performance of the ACC-PT Organohydrogels: The adhesion tests were performed using the lap shear test with the wick/Roell Z020 universal tester instrument. The ACC-PT organohydrogel with 10 × 10 × 1 mm was placed between two substrates (including glass, aluminum, steel, copper, iron, plastic, and pig skin)) and compressed with a 50 g weight for 60 s, then pulled to separate the two substrates at a rate of 10 mm min^{-1}. When the cohesion

or adhesion of the gel failed, we would get the maximum tensile force. The fracture tensile forces divided the areas of organohydrogel and gave rise to the value of the adhesive strength.

Differential Scanning Calorimetry (DSC) Tests: Samples (6–10 mg) were added in aluminum pans and transferred to a DSC system (DSC, 2500). The samples were cooled from 30 to −120 ºC at a rate of −10 ºC min^{-1}, held at −120 ºC for 5 min, and warmed back to 30 ºC at a rate of 10 ºC min^{-1}. The heat flow during the cooling and warming processes was monitored in real-time.

Raman Tests: Raman spectra were obtained on a Raman spectrometer (HORIBA Scientific LabRAM HR Evolution) at an excitation wavelength of 532 nm.

Water Retention Tests: The prepared AC hydrogel, ACC hydrogel, and ACC-PT organohydrogel were placed in the laboratory at room temperature, and the sample weights were measured daily at regular times. W/W_0 was calculated for different samples, where W means the weight of hydrogel samples measured on the same day, and W_0 means the weight of hydrogel samples measured on the first day.

Equilibrium welling Ratios: The prepared AC hydrogel, ACC hydrogel, and ACC-PT organohydrogel were swollen in distilled water until reaching an equilibrium at room temperature. Subsequently, the swelled samples were taken out from the distilled water and immediately weighed after sucking off the surface water with filter paper. The equilibrium swelling ratio was calculated according to equation (1):

$$Equilibrium\ swelling\ ratio(\%) = \frac{W_w - W_0}{W_0} \quad (1)$$

In addition, the swelling ratio of the samples at different times was also recorded and calculated during the process.

Antibacterial Tests: The antibacterial performance of the coatings was investigated via E. coli and S. aureus with the LB plate method. First of all, bacterial suspension was prepared in Luria–Bertani (LB) media to about 10^8 CFU/mL for 24 h. The coated glass slides were immersed in 20 ml bacterial suspension above and incubated in a constant temperature at 37 ℃ for 24 h. Then these slides were taken out, washed slightly with sterile PBS to remove the weakly attached bacteria, placed in 20 ml sterile PBS, and sonicated for 15 min. Finally, the sonicated liquid was diluted 10000 times and inoculated on LB medium at 37 ℃ for 24 h. The formation of colonies on LB was observed to judge the antibacterial performance of the coating.

Mechanical Property Tests:

(1) **Tensile Tests:** A tensile test was performed by using a wick/Roell Z020 universal tester instrument equipped with a 50 N load cell at a speed of 10 mm·min^{-1}. The tensile properties of AC hydrogel, ACC hydrogel, and ACC-PT organohydrogel (Ca^{2+}= 0.005, 0.075, 0.1, 0.2 mol/L) were tested. Five samples were tested for each hydrogel. A tensile experiment was carried out at room temperature (25 ℃) with samples of the dog bone shape (35 mm×2 mm×1mm). For cyclic tensile test, the ACC-PT organohydrogels were stretched or compressed to a certain strain and recovered for ten cycles without cessation. Due to its anti-freezing properties, we also evaluated the mechanical performance of ACC-PT organohydrogel at −40 °C, and the test conditions were the same as those above.

(2) **Compressive Tests:** The cylindrical samples with a height of 7.0 mm and a diameter of 30 mm were compressed until they fractured at a rate of 10 mm min $^{-1}$.

Conductivity: The ionic conductivity of the ACC-PT organohydrogel was measured by a two-probe AC impedance method via an electrochemical workstation (CHI660e). The samples were sandwiched between two copper electrodes and measured at frequencies ranging from 0.01 to

10^5 Hz with an oscillating amplitude of 5 mV. The ionic conductivity σ (S/m) of ACC-PT organohydrogel at different temperatures was calculated by the following equation (2):

$$\sigma = \frac{L}{S \times R} \quad (2)$$

where L (m) is the distance between the two electrodes, S (m^2) is the cross-sectional area of the hydrogels, and R (Ω) is the resistance acquired from Nyquist plots. The ionic conductivity of the ACC-PT organohydrogel at different temperatures was measured using a Peltier temperature control unit.

Potential Demonstrations of the e-skins

(1) **Wearable Strain Sensors:** The electrical signals of the hydrogels were recorded by an electrochemical workstation (CHI660e). In the room temperature test, the prepared ACC-PT organohydrogel was connected to flexible copper electrodes at both ends to assemble an e-skin, which was attached to the human body to detect various strain signals in real time at a constant voltage of 1 V. The e-skin was then attached to the human body to detect the strain signals in real time. For low-temperature testing, the e-skins were placed on a cooling platform at −78 °C for 6 h. Afterward, e-skins were attached to the knuckles of the robotic hand, and object grasping experiments were carried out, grasping oranges, eggs, apples, and cups, and the signal changes when the sensor grasped different objects were recorded. Relative changes in resistance were calculated as the following equation (3):

$$\frac{\Delta R}{R_0} = \frac{R - R_0}{R_0} \times 100\% \quad (3)$$

where R_0 and R are the original resistance at the strain of 0% and the real-time resistance, respectively.

The sensitivity of the organohydrogel with an increase in strain was investigated. The

sensitivity defined as the gauge factor was calculated by the equation (4):

$$GF = \frac{\Delta R/R_0}{\varepsilon} \quad (4)$$

The participants for the real-life test for organohydrogel-based sensors were the authors (S.Z and R.S) of this article, who took part following informed consent and have provided informed consent. Ethical approval was not required for this work.

(2) **Pressure-Sensing Performance:** The ACC-PT organohydrogel was prepared as a cylinder with a cylinder with a height of 7 mm and a diameter of 30 mm. The samples were sandwiched between two copper electrodes and connected to an electrochemical workstation (CHI660E), where different pressures were applied, and the signal changes during the process were recorded to verify the pressure-sensitive properties of the hydrogel. Relative changes in current was calculated as the following equation (5):

$$\frac{\Delta I}{I_0} = \frac{I - I_0}{I_0} \times 100\% \quad (5)$$

The sensitivity of the organohydrogel with an increase in pressure was investigated. The sensitivity defined as the gauge factor was calculated by the equation (6):

$$S = \frac{(I - I_0)/I_0}{\delta P} = \frac{\Delta I/I_0}{\delta P} \quad (6)$$

A 3×3 pixel array was formed by nine ACC-PT organohydrogel pressure-sensitive sensor units (each 0.5×0.5 cm ^{2}) and encapsulated with VHB. The array was placed at −78 °C for 6 h. Subsequently, a 1 kg weight was placed on the array sensors at −78 °C, and the response current signal was recorded.

(3) Wearable Smart Gloves for Distinguishing Gestures

At −40 °C, five independent e-skins were installed into the joints of each finger (thumb, index

finger, middle finger, ring finger, and little finger) of the glove, and then different gestures such as "OK", "Ye" and "Six" were made by the fingers. The sensor signal changes during the process are monitored in order to recognize different gestures.

(4) E-Skins for Human-Machine Interaction for Exploration at −78 °C

A wireless Bluetooth transmission system that can be connected to an e-skin was developed, and the wireless component was integrated with an ACC-PT organohydrogel-based e-skin for motion and pressure sensing at low temperatures. The e-skin was affixed on the finger joints of a robotic hand, and silver wires were selected as the electrode layer and encapsulated with copper foil tape on both sides. The motion signals from the e-skin were converted to current signals by applying a 1 V voltage through a removable power supply at −78 °C and further modulated using a microcontroller. These processed signals are transmitted wirelessly via a Bluetooth module to a dedicated mobile application called "Bluetooth Debugger". The mobile application visualizes the changes in current and enables the wireless transmission of the signals.

Statistical analysis: All data were obtained from three or five repeated measurements. FTIR data was processed by OMNIC, XPS data was processed by Avantage, EDS data was processed by Phenom Element, and AFM data was processed by Gwyddion. All graphs and data analysis were performed using Adobe Photoshop 2022 and OriginPro 2019 Software.

2. Supplementary Table

Table 1. Overview of anti-freezing ability, conductivity, sensitivity, and tensile strain with reported glycerol-water binary solvent organohydrogels.

Number	Solvent	Antifreezing	Conductivity	Sensitivity	Tensile	Ref.

		temp. (°C)	(S/m)	(GF)	strain	
1	Glycerol-water	-103	1.57 (Ca^{2+}=0.075mol/L)	6.47	1700%	This work
2	Glycerol-water	-50.08	-	1.34mv·kPa^{-1}	780%	[1]
3	Glycerol-water	-	0.044	1.7	1112%	[2]
4	Glycerol-water	-50	0.011	-	2780%	[3]
5	Glycerol-water	-20	0.7	0.25	600%	[4]
6	Glycerol-water	-80	-	-	688%	[5]
7	Glycerol-water	-80	1.314 (Na^{+}=1.7mol/L)	8.303	1002%	[6]
8	Glycerol-water	-63.7	0.72	1.02	220%	[7]
9	Glycerol-water	-36.3	0.09	5.82	247%	[8]

Table 2. The ratio of samples fed into the system.

Samples	AM /mmol	CMC /mmol	$CaCl_2·2H_2O$ /mmol	C_{18} /mmol	PEI-TA /g	H_2O /vol%	Glycerol /vol%
AC	39.95	1.24	1.50	0	0	100	0
ACC	39.95	1.24	1.50	0.52	0	100	0
ACC-PT	39.95	1.24	1.50	0.52	2	50	50

Table 3. Overview of ionic tensile strain, conductivity, sensitivity, anti-freezing ability, and adhesiveness with state-of-the-art reported stretchable hydrogels.

Number	Gel systems	Tensile strain	Conductivity (S/m)	Sensitivity (GF)	Antifreezing temp. (°C)	Adhesiveness	Ref.
1	PAM- C_{18}-CMC-Ca^{2+}-PEI-TA	1700%	1.57 (Ca^{2+}=0.075mol/L)	6.47	-103	42.76 kPa	This work
2	Gelatin/nanofibrillated cellulose/Fe^{3+}	70%	4.8×10^{-5}	0.67	-60	-	[9]
3	PDA@CNT/PAM	730%	0.02	3.93	-	25.60 kPa	[10]

4	ChCl-LA-ACAD	800%	0.0011	3.83	-	-	[11]
5	DA-PPy/PVA	370%	0.06	3.40	-	-	[12]
6	PV/KI/glycerol	1112%	0.044	1.70	-	-	[2]
7	Ana-AMPSNa	6185%	1.3	2.6	-78	27.80 kPa	[13]
8	PVA/PEDOT:PSS	600%	0.16	3.93	-	-	[14]
9	BC/PPy@EF	519%	-	4.86	-	-	[15]
10	PAM–HA–Zn^{2+}	3040%	0.44	3.79	-	25.50 kPa	[16]
11	P(AM/AA)/Trehalose/ LiCl	4529%	4.1 (Li^{+} = 20 wt%)	3.59	-20	26.65 kPa	[17]
12	(PAM–CMC)/Ca	1480%	1.4	1.42	-	-	[18]
13	PVA/PA/ CNCs@PDDA	514%	0.6	0.9	-38	-	[19]
14	chitosan/PAM	620%	2.361	-	-30	-	[20]
15	PVA/alginate gel	750%	-	1.5	-	-	[21]
16	PAM/PVA-glycerol	2780%	0.011	-	-50		[3]
17	PVA-CNFs	660%	3.2	1.5	-70	-	[22]
18	Gelatin/PAA (NaCl/Gly/W)	600%	0.7	0.25	-20	-	[4]
19	Gelatin (Citrate/Gly/W)	688%			-80	105	[5]
20	Cellulose (NaCl/Gly/W)	220%	0.72	1.02	-63.7	-	[7]
21	PVA/PAM (NaCl/Gly/W)	2333%	1.24×10^{-4}	-	-50	-	[23]
22	PVA/Mxene ($ZnSO_4$ /Gly/W)	247%	0.09	5.82	-36.3		[8]

Table 4. Comparison of sensitivity and detection threshold with reported pressure sensors.

Number	Gel systems	LOD(kPa)	Sensitivity (S)	Ref.

1	PAM- C_{18}-CMC-Ca^{2+}-PEI-TA	0.005	0.32 kPa^{-1} (0-10kPa)	This work
2	Gelatin/nanofibrillated cellulose/Fe^{3+}	20	0.0126 kPa^{-1} (20-100kPa)	9
3	PDA@CNT/PAM	0.1	0.0393 kPa^{-1}	10
4	CNT@PU	5.31	0.2740 kPa^{-1} (5.31 - 21.25 kPa)	24
5	Def-ZIF-8/PPY/BC	-	0.0644 kPa^{-1} (＜2 kPa)	25
6	P(MAA-AM) /AgNPs	6	-	26
7	P(AA-co-MLA)-ODex/Fe^{3+}	-	0.55 kPa^{-1} (0-0.1 kPa) 0.12 kPa^{-1} (0.1-2 kPa) 0.02 kPa^{-1} (> 2 kPa)	27
8	PAAm-NaCl hydrogel	0.035	0.24 kPa^{-1} (＜70 kPa)	28
9	SBS/AgNP	-	0.21 kPa^{-1} (<2 kPa) 0.064 kPa^{-1} (2-10 kPa)	29
10	(PAA-r-BVIT)/PEO	-	0.22 kPa^{-1} (0-1.4 kPa) 0.13 kPa^{-1} (1.4 -4.7 kPa) 0.07 kPa^{-1} (4.7-8 kPa)	30
11	GelMA hydrogel	0.0001	0.19 kPa^{-1} (0-1.2 kPa) 0.02 kPa^{-1}	31

			(1.6-5 kPa)	
12	Fe^{3+} /PAA-PVA IPN	1.55	~ 0.018 kPa^{-1} (0-100 kPa)	32
13	ACC/PAA/alginate mineral hydrogel	-	0.17 kPa^{-1} (0-1 kPa)	33
14	PAAm/TEMED-NaCl hydrogel	-	0.267 kPa^{-1} (< 3.45 kPa) 0.0757 kPa^{-1} (3.45-12 kPa)	34

3. Supplementary Figures

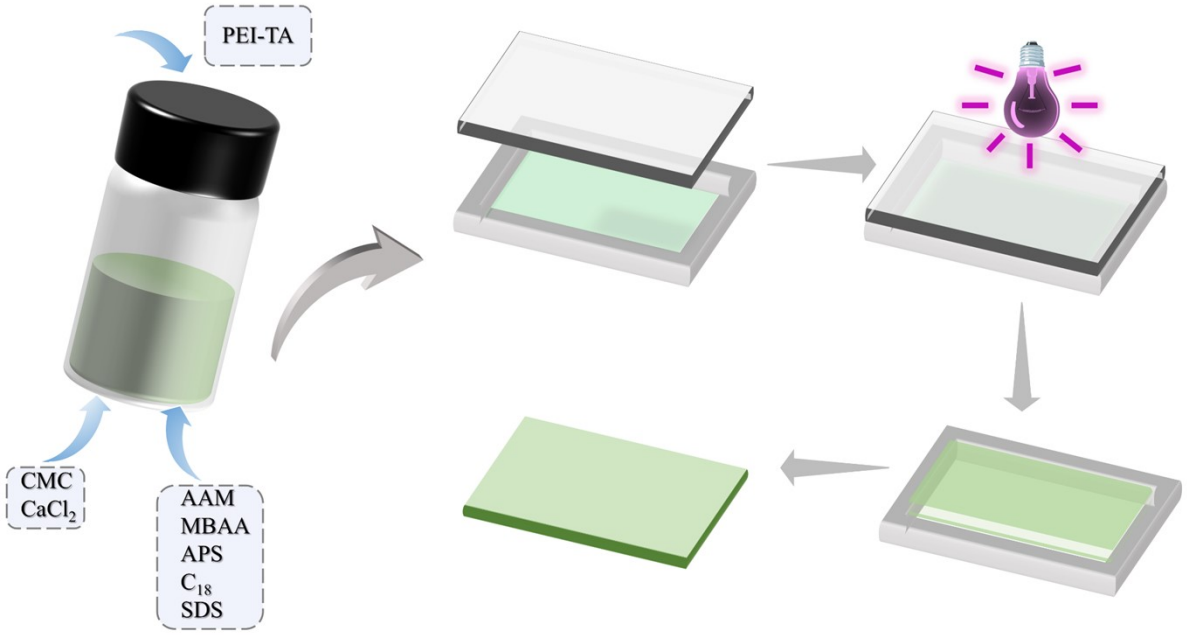

Figure S1. Preparation of ACC-PT organohydrogel.

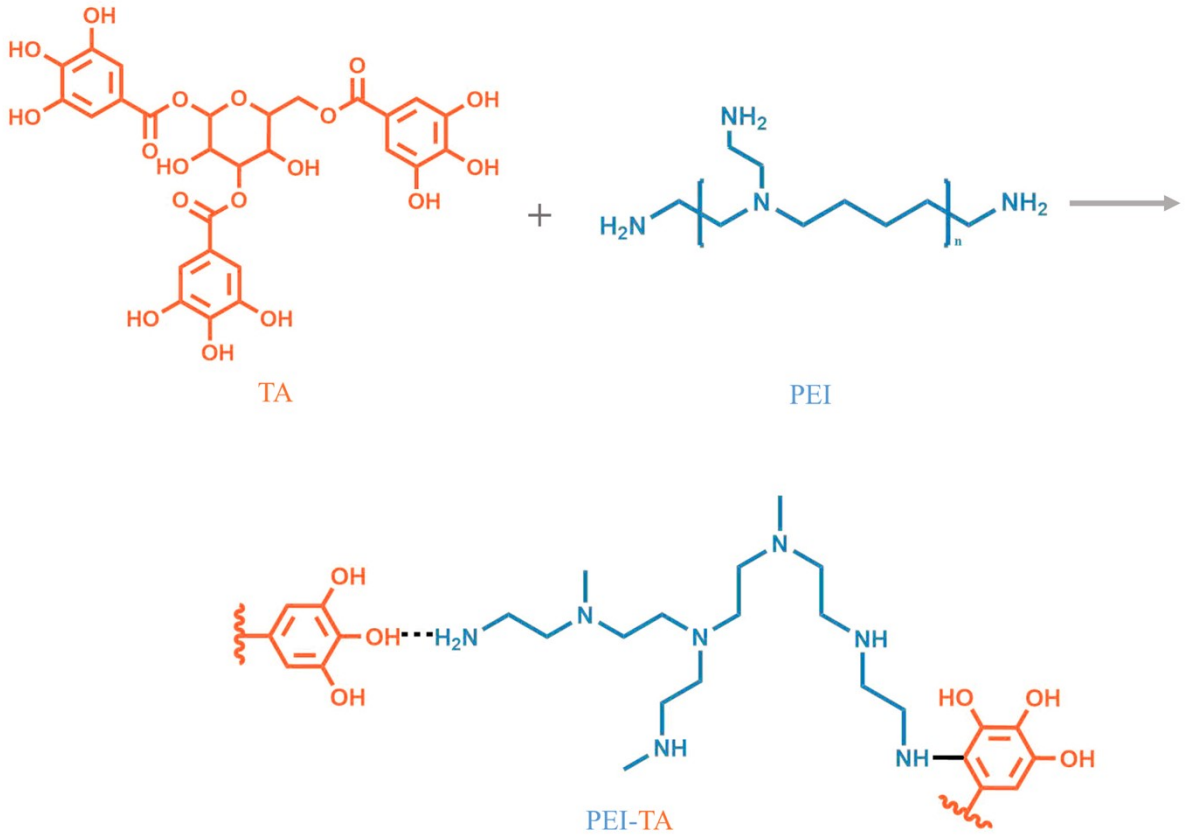

Figure S2. Synthesis diagram of PEI-TA.

Both PEI and TA possess broad-spectrum bactericidal properties and show great potential for medical applications. We evaluated the antibacterial properties of AC, ACC hydrogels, and ACC-PT organohydrogel against Gram-negative *E. coli* and Gram-positive *S. aureus*. It can be observed that with the addition of PEI-TA bionic binder, the ACC-PT organohydrogel showed the best antibacterial performance, with 99.19% (*E. coli*) and 97.70% (*S. aureus*), respectively, compared to the control group. The antibacterial performance was derived from the inherent antibacterial advantages of PEI and TA, whereby protonated amines in PEI can bind to the surface of the cell membrane with negatively charged components on the surface of the cell membrane, leading to cell membrane rupture and bacterial death. [35]The catechol moiety in TA, on the other hand, can bind to the negatively charged bacterial cell surface, leading to bacterial death.[36]

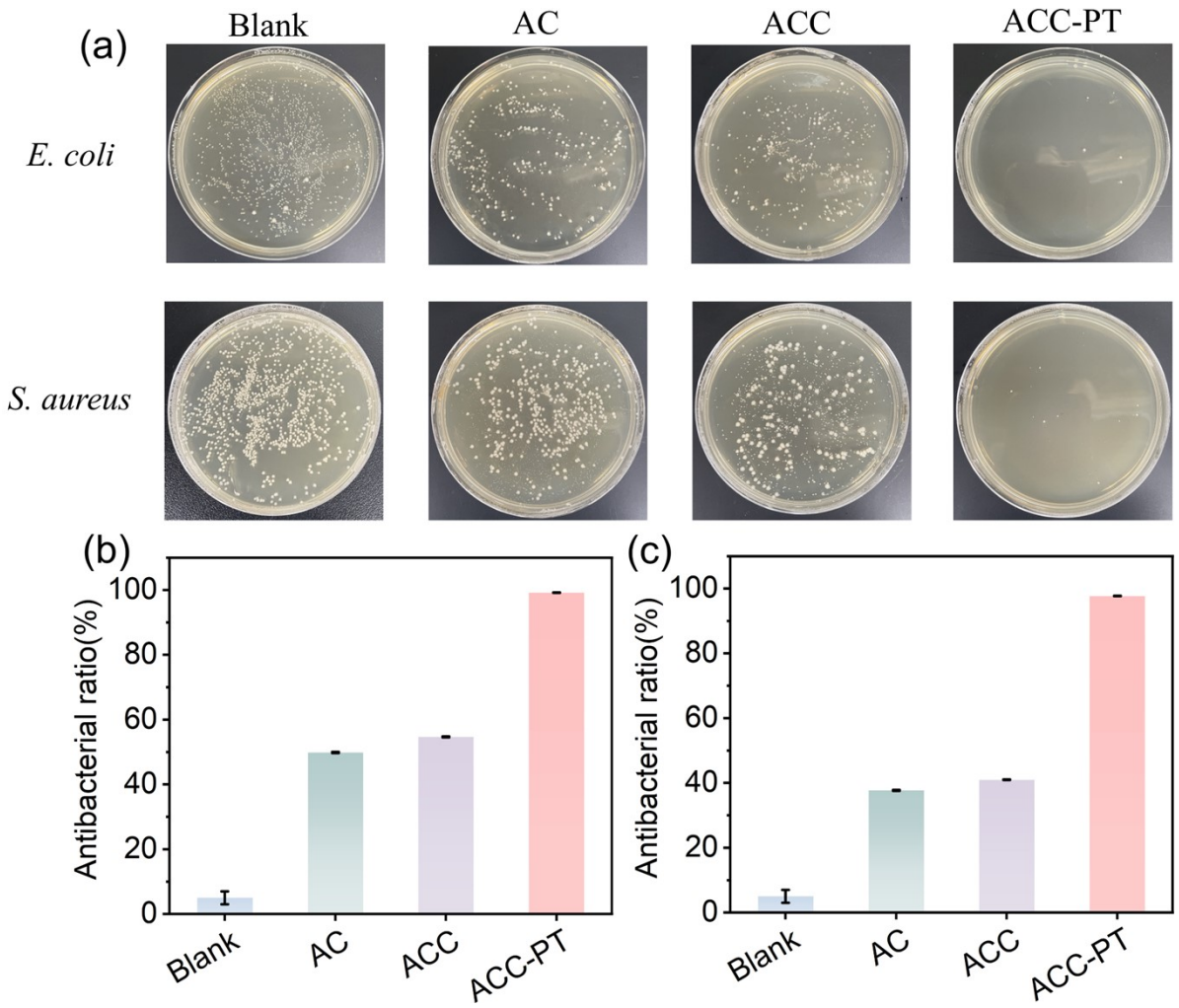

Figure S3. (a) Photographs of surviving *E. coli* and *S. aureus* on agar medium showing the in vitro antibacterial performance of AC, ACC, and ACC-PT, respectively. (b) Antibacterial rates of control samples and AC, ACC, and ACC-PT.

FTIR in Figure S4 shows the successful synthesis of PEI-TA. The absorption peaks appearing at 1713 cm^{-1} and 3392 cm^{-1} can be attributed to the vibration of C=O in TA, and the absorption peaks at 2948 cm^{-1} and 3353 cm^{-1} are attributed to $-CH_2$ and $-NH_2$ in PEI, proving the successful polymerization of PEI-TA. Meanwhile, the absorption peaks of $-OH$ and $-NH_2$ shifted to 3353 cm^{-1} also proved the formation of strong hydrogen bonds between PEI and TA. Moreover, it was observed that the absorption peak at 1506 cm^{-1} was significantly increased,

which is the result of the Michael addition reaction of the $-NH_2$ of PEI and the benzene ring of TA.[37, 38]

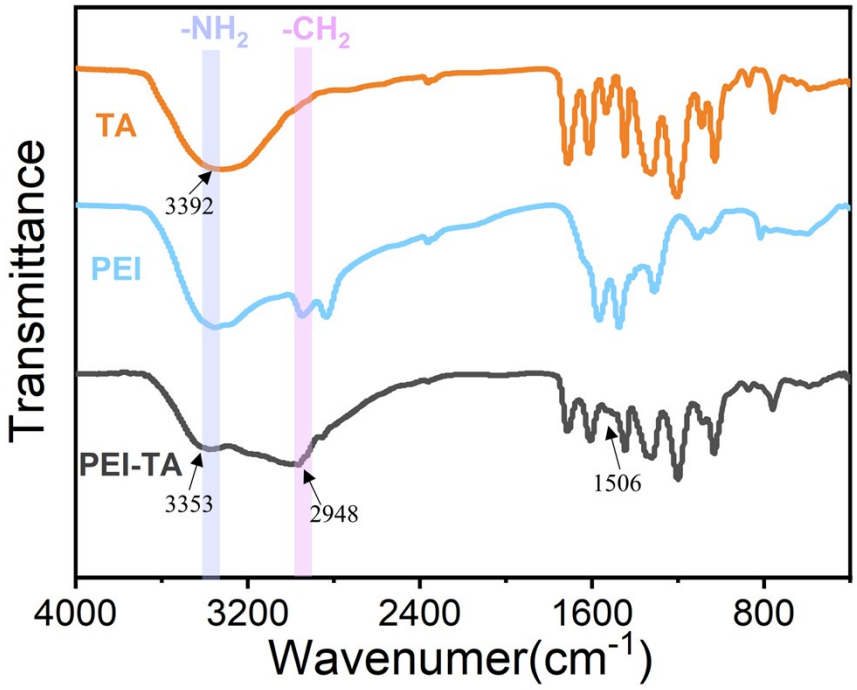

Figure S4. FTIR spectra of TA, PEI, and PEI-TA.

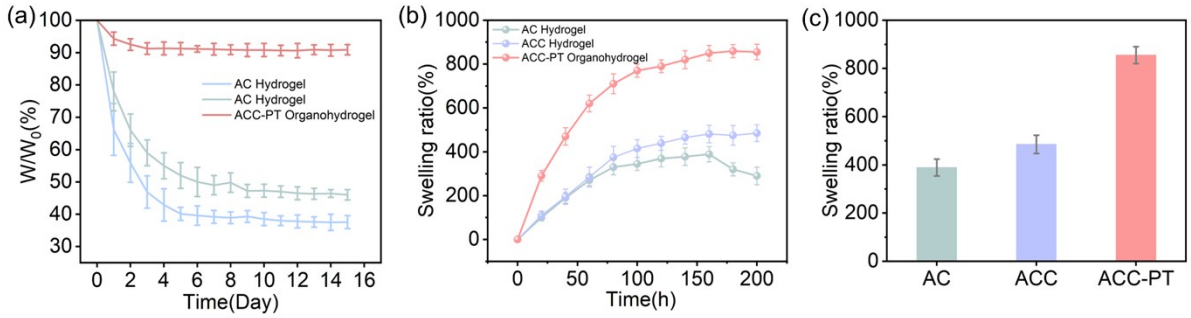

Figure S5. (a)W/W_0 of AC hydrogel, ACC hydrogel, and ACC-PT organohydrogel after different days at room temperature. (b) Swelling curves and equilibrium swelling ratios of AC hydrogel, ACC hydrogel, and ACC-PT organohydrogel.

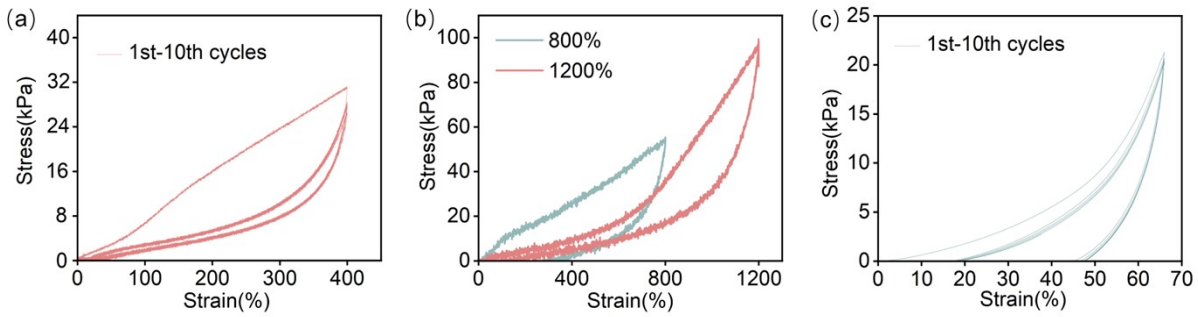

Figure S6. ACC-PT organohydrogel (a) 10 loading-unloading tensile cycles at 400% strain and (b) loading-unloading tensile tests at 800 and 1200% large strains and (c) 10 loading-unloading compression cycles at 65% compressive strain.

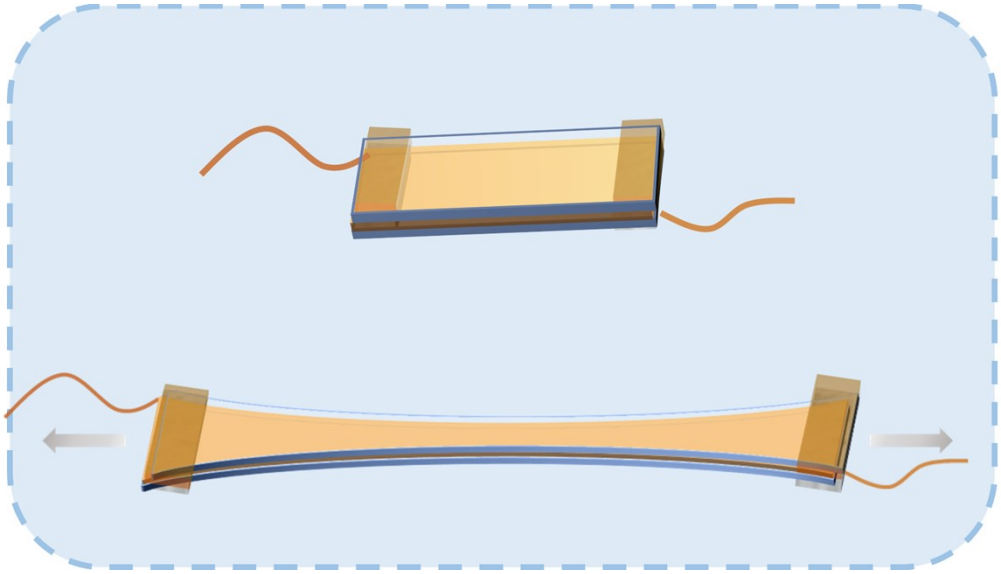

Figure S7. Schematic diagram of strain sensor stretching process based on ACC-PT organohydrogel

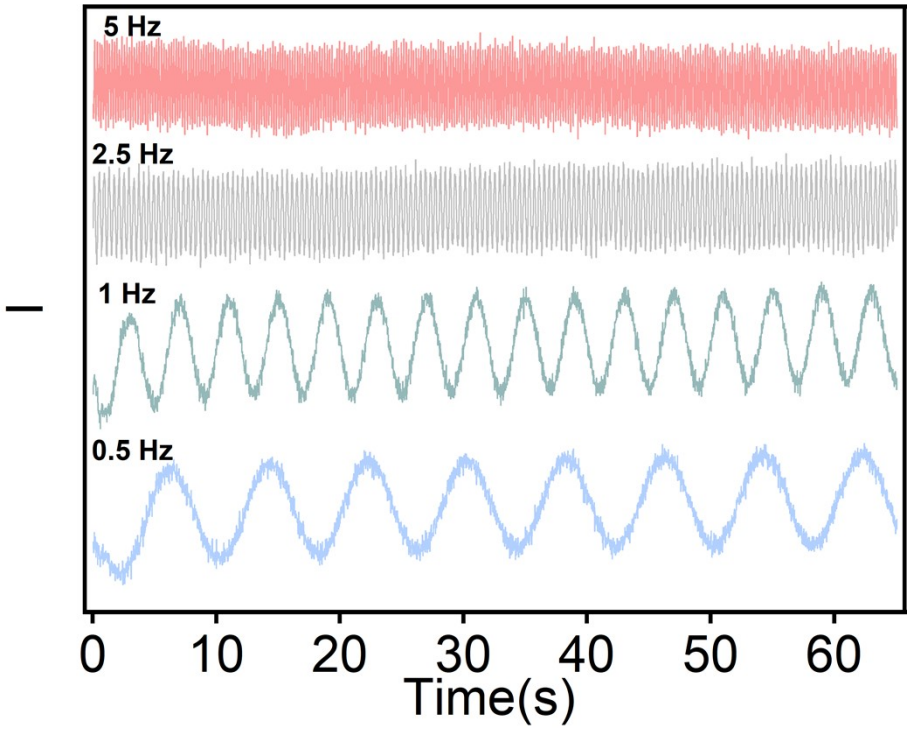

Figure S8. Relative current signal variations at different frequencies for a certain tensile stress of ACC-PT organohydrogel-based strain sensor.

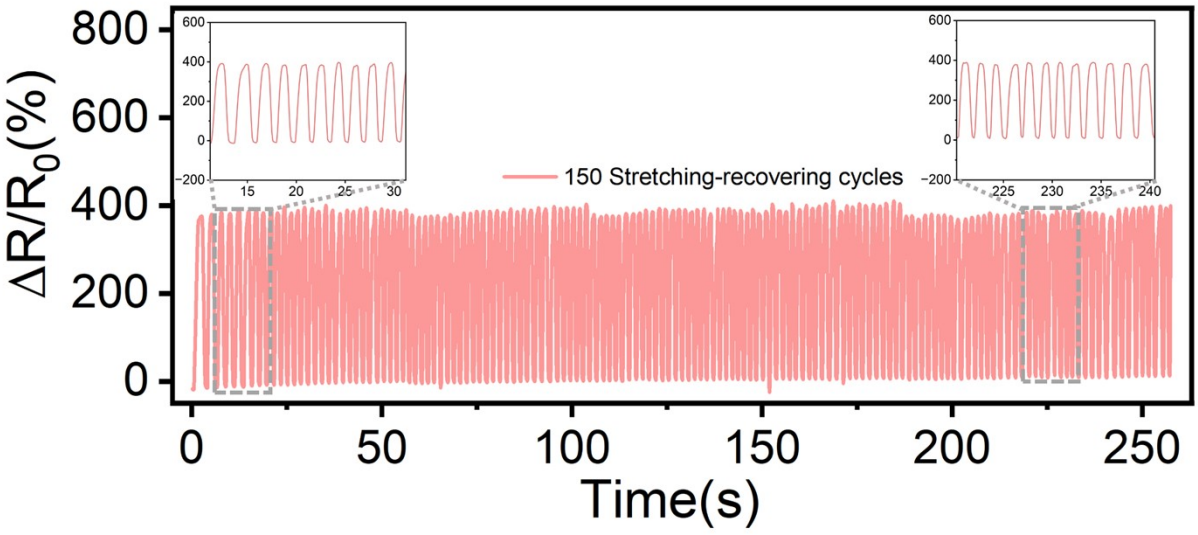

Figure S9. Relative resistance variations for 150 cycles of loading-unloading at 250% tensile strain.

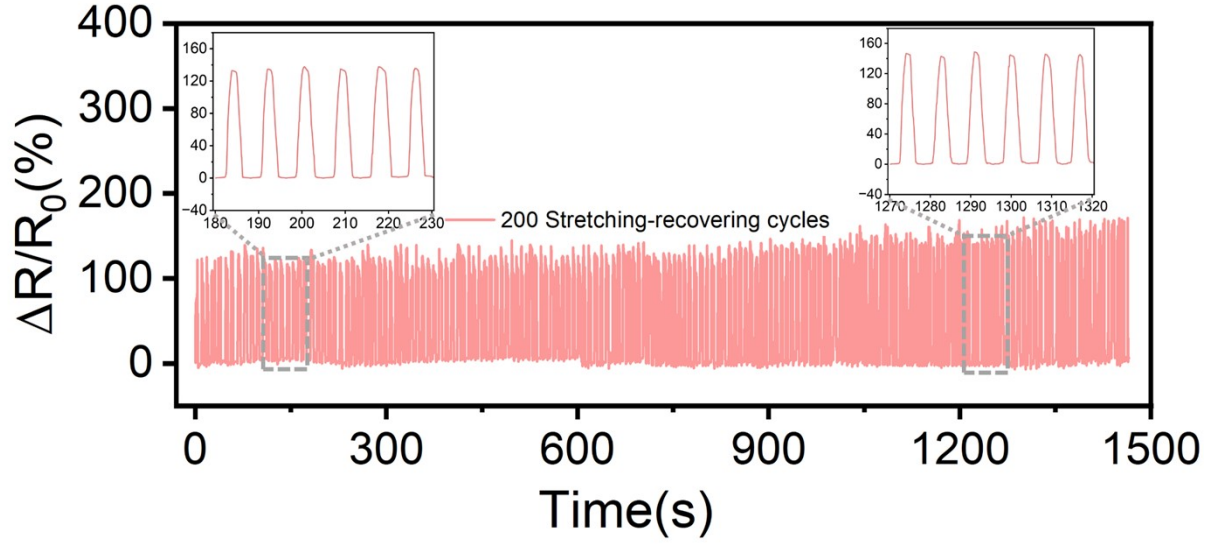

Figure S10. Relative resistance variations for 200 cycles of loading-unloading at 100% tensile strain.

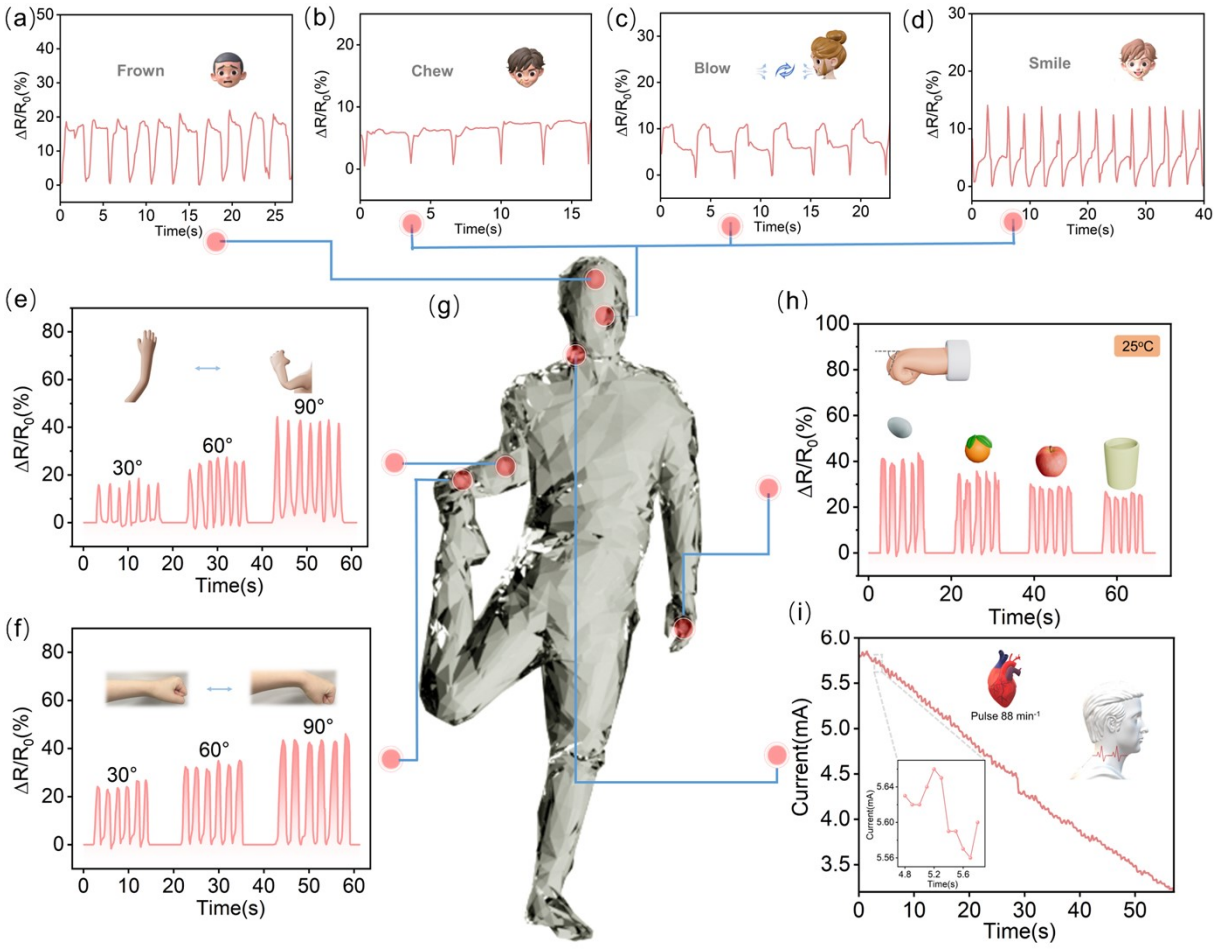

Figure S11. Real-time motion monitoring with strain sensors based on ACC-PT organohydrogel. Facial sensing signals for (a) frowning and (b) chewing and (c) blowing and

(d) smiling. Human motion sensing signals (e) elbow flexion and (f) wrist flexion and (g) schematic diagram of human motion and physiological signal monitoring and (h) grasping eggs, oranges, apples, cups of water. Physiological signal monitoring (i) signals of real-time current in response to neck pulse.

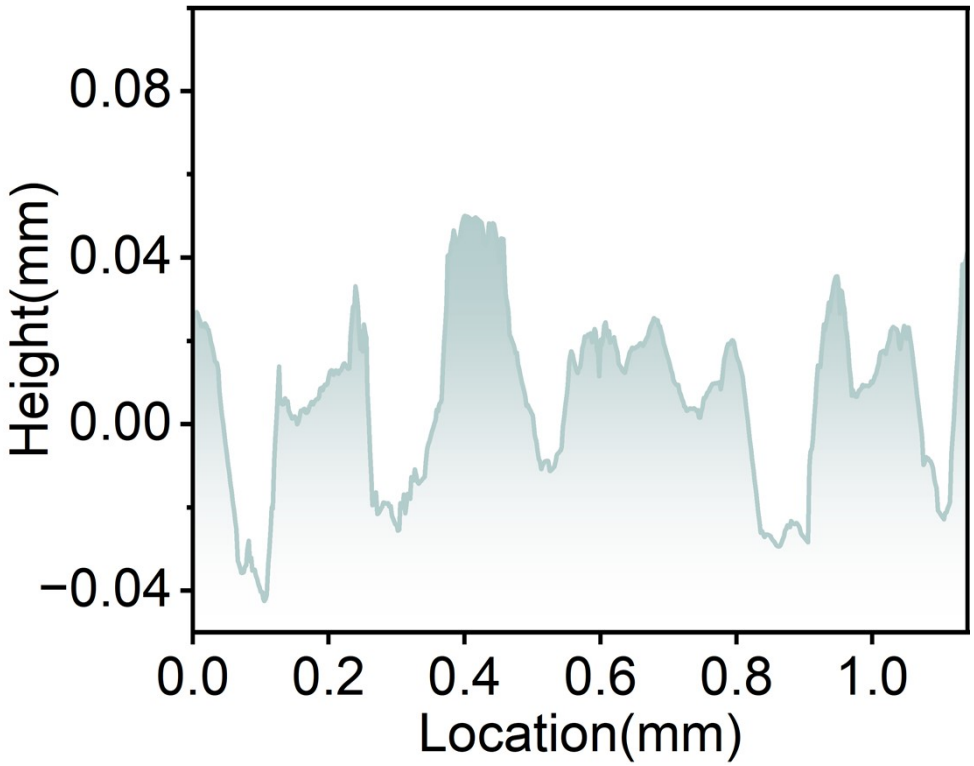

Figure S12. Roughness scanning of ACC-PT organohydrogel surface.

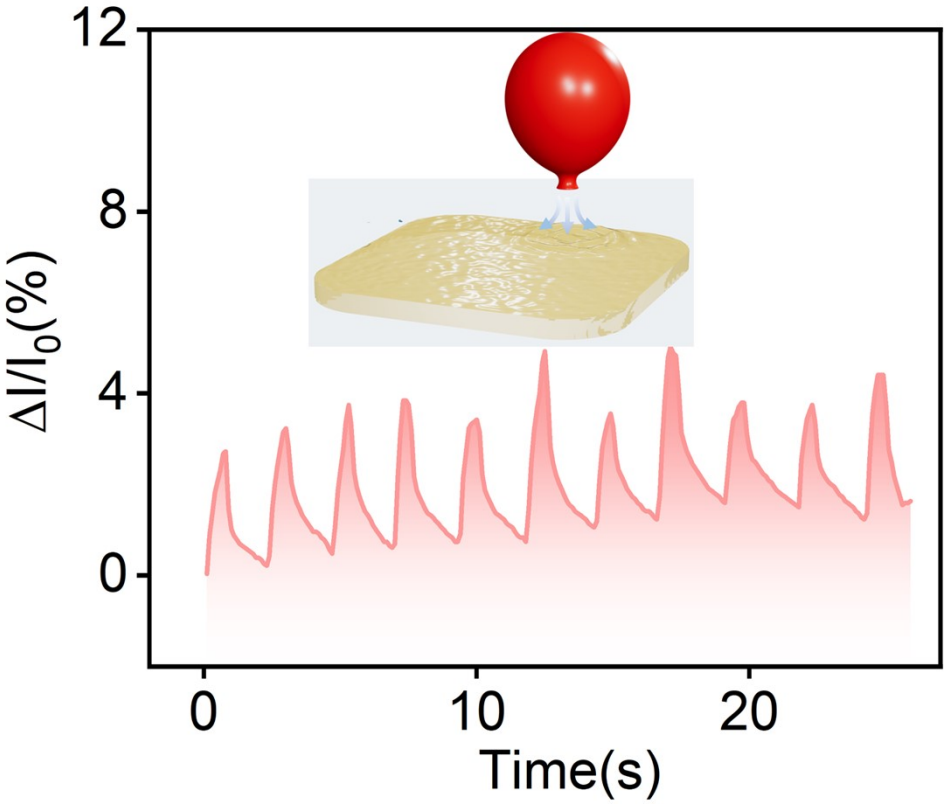

Figure S13. Sensing performance of the flexible electronic sensor to airflow. Inset: the image of the airflow generated from the rubber suction bulb to the sensor.

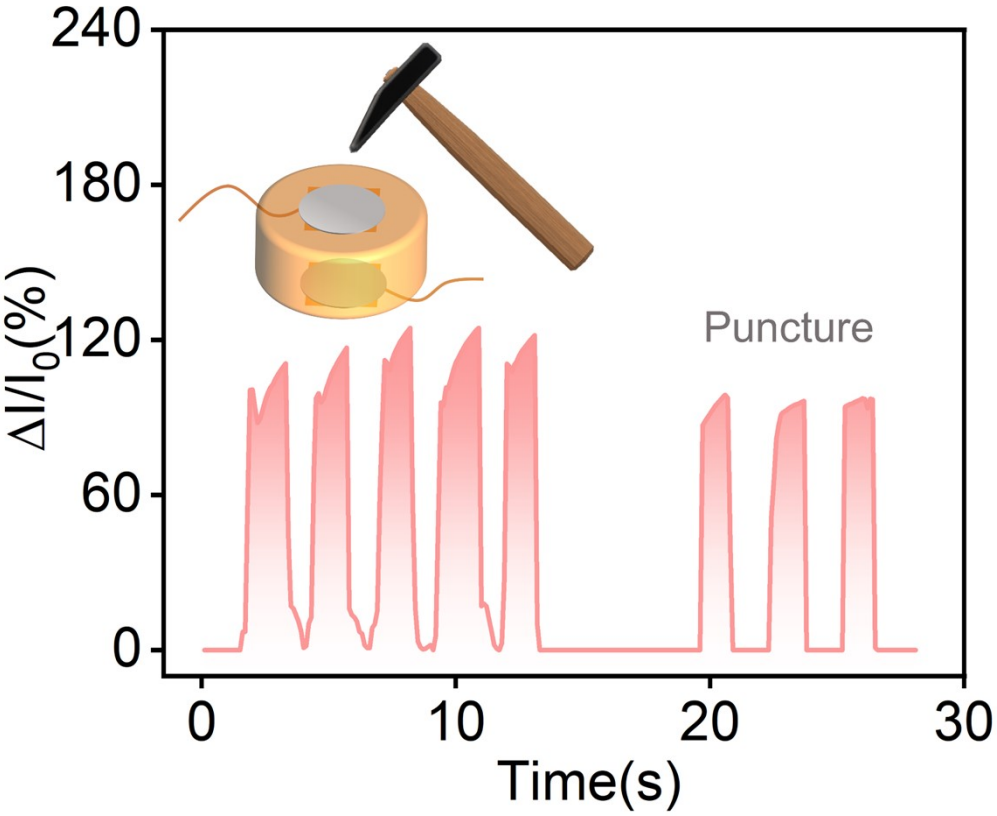

Figure S14. Sensing performance of the flexible electronic sensor for hammering and

puncturing. Illustration: Image of a sensor struck by a hammer.

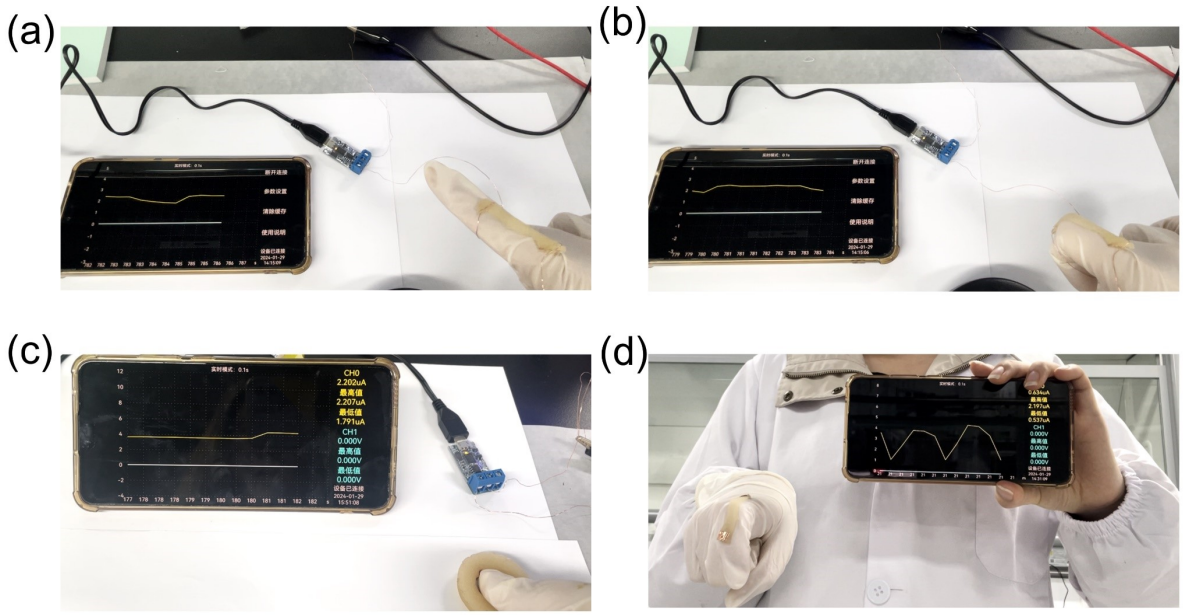

Figure S15. The ACC-PT organohydrogel-based e-skin demonstrates exceptional pressure and tension sensitivity at ambient temperature.

4. References

1. Y. Shi, Y. Guan, M. Liu, X. Kang, Y. Tian, W. Deng, P. Yu, C. Ning, L. Zhou, R. Fu and G. Tan, *ACS Nano*, 2024, **18**, 3720-3732.
2. Y. Wang, Y. Wu, Y. Liu, H. Wu, W. Xiao, H. Zhang, X. Huang, J. Zhang, H.-G. Xue and J.-f. Gao, *ACS Mater. Lett.*, 2024, **6**, 1140-1150.
3. Y. H. Wu, Y. J. Mu, Y. Luo, C. Menon, Z. W. Zhou, P. K. Chu and S. P. Feng, *Adv. Funct. Mater.*, 2022, **32**, 2110859.
4. L. Y. Fang, J. C. Zhang, W. J. Wang, Y. L. Zhang, F. Chen, J. H. Zhou, F. B. Chen, R. Li, X. C. Zhou and Z. Xie, *ACS Appl .Mater. Interfaces*, 2020, **12**, 56393-56402.
5. Z. H. Qin, D. Y. Dong, M. M. Yao, Q. Y. Yu, X. Sun, Q. Guo, H. T. Zhang, F. L. Yao and J. J. Li, *ACS Appl .Mater. Interfaces*, 2019, **11**, 21184-21193.
6. J. Huang, S. Peng, J. Gu, G. Chen, J. Gao, J. Zhang, L. Hou, X. Yang, X. Jiang and L. Guan, *Mater. Horiz.*, 2020, **7**, 2085-2096.
7. Y. L. Guo, N. Liu, Q. Cao, X. Cheng, P. Zhang, Q. Q. Guan, W. Zheng, G. M. He and J. X. Chen, *Acs*

Applied Polymer Materials, 2022, **4**, 6202-6210.

8. Y. B. Feng, H. Liu, W. H. Zhu, L. Guan, X. T. Yang, A. V. Zvyagin, Y. Zhao, C. Shen, B. Yang and Q. Lin, *Adv. Funct. Mater.*, 2021, **31**, 2105264.
9. H. Fu, B. Wang, J. Li, D. Cao, W. Zhang, J. Xu, J. Li, J. Zeng, W. Gao and K. Chen, *Mater. Horiz.*, 2024, **11**, 1588-1596.
10. Y. Li, D. Yang, Z. Wu, F.-L. Gao, X.-Z. Gao, H.-Y. Zhao, X. Li and Z.-Z. Yu, *Nano Energy*, 2023, **109**, 108324.
11. W. Xu, T. Shen, Y. Ding, H. Ye, B. Wu and F. Chen, *Small*, 2024, **23**, 10072.
12. S. Chen, B. Guo, J. Yu, Z. Yan, R. Liu, C. Yu, Z. Zhao, H. Zhang, F. Yao and J. Li, *Chem. Eng. J.*, 2024, **486**, 150182.
13. X. Huang, Z. Zheng, H. Wang, W. Xu, M. Wu, M. Wang, C. Chen, L. Wan, R. Du, T. Zhu, Z. Huang, X. Wang, X. Wang, Q. Zhang and X. Jia, *Adv. Funct. Mater.*, 2024, **34**, 2312149.
14. Z. Zhang, G. Chen, Y. Xue, Q. Duan, X. Liang, T. Lin, Z. Wu, Y. Tan, Q. Zhao, W. Zheng, L. Wang, F. Wang, X. Luo, J. Xu, J. Liu and B. Lu, *Adv. Funct. Mater.*, 2023, **33**, 2305705.
15. C. Gao, Y. Liu, F. Gu, Z. Chen, Z. Su, H. Du, D. Xu, K. Liu and W. Xu, *Chem. Eng. J.*, 2023, **460**, 141769.
16. S. Guan, C. Xu, X. Dong and M. Qi, *J. Mater. Chem. A*, 2023, **11**, 15404-15415.
17. H. Cai, D. Zhang, H. Zhang, M. Tang, Z. Xu, H. Xia, K. Li and J. Wang, *Chem. Eng. J.*, 2023, **472**, 144849.
18. J. Bai, R. Wang, X. Wang, S. Liu, X. Wang, J. Ma, Z. Qin and T. Jiao, *Cell Reports Physical Science*, 2021, **2**, 100623.
19. Y. Nie, D. Yue, W. Xiao, W. Wang, H. Chen, L. Bai, L. Yang, H. Yang and D. Wei, *Chem. Eng. J.*, 2022, **436**, 135243.
20. S. W. Huang, L. Hou, T. Y. Li, Y. C. Jiao and P. Y. Wu, *Adv. Mater.*, 2022, **34**, 2110140.
21. W. Cui, Y. Zheng, R. J. Zhu, Q. F. Mu, X. Y. Wang, Z. S. Wang, S. Q. Liu, M. Li and R. Ran, *Adv. Funct. Mater.*, 2022, **32**, 2204823.
22. Y. Ye, Y. Zhang, Y. Chen, X. Han and F. Jiang, *Adv. Funct. Mater.*, 2020, **30**, 2003430.
23. Y. H. Wu, J. K. Qu, X. H. Zhang, K. L. Ao, Z. W. Zhou, Z. Y. Zheng, Y. J. Mu, X. Y. Wu, Y. Luo and S. P. Feng, *Acs Nano*, 2021, **15**, 13427-13435.
24. J. Liao, X. Dai, J. Han, J. Yang, Y. Wu, Y. Cao, Y. Qiu, Y. Wang, L.-B. Huang, H. Ni and W. Feng,

Nano Energy, 2024, **121**, 109252.

25. Y. Men, Z. Qin, Z. Yang, P. Zhang, M. Li, Q. Wang, D. Zeng, X. Yin and H. Ji, *Adv. Funct. Mater.*, 2024, **34**, 2316633.
26. R. Zhao, J. Luo, T. Ke, J. Zhang, D. Astruc, J. Zhou and H. Gu, *Chem. Eng. J.*, 2024, **485**, 149816.
27. Y. Chen, S. Dai, H. Zhu, H. Hu, N. Yuan and J. Ding, *New J. Chem.*, 2021, **45**, 314-320.
28. Z. Q. Shen, X. Y. Zhu, C. Majidi and G. Y. Gu, *Adv. Mater.*, 2021, **33**, 2102069.
29. J. Lee, H. Kwon, J. Seo, S. Shin, J. H. Koo, C. Pang, S. Son, J. H. Kim, Y. H. Jang, D. E. Kim and T. Lee, *Adv. Mater.*, 2015, **27**, 2433-2439.
30. A. Wang, Y. F. Wang, B. Zhang, K. N. Wan, J. X. Zhu, J. S. Xu, C. Zhang and T. X. Liu, *Chem. Eng. J.*, 2021, **411**, 128506.
31. Z. Li, S. Zhang, Y. Chen, H. Ling, L. Zhao, G. Luo, X. Wang, M. C. Hartel, H. Liu, Y. Xue, R. Haghniaz, K. Lee, W. Sun, H. Kim, J. Lee, Y. Zhao, Y. Zhao, S. Emaminejad, S. Ahadian, N. Ashammakhi, M. R. Dokmeci, Z. Jiang and A. Khademhosseini, *Adv. Funct. Mater.*, 2020, **30**, 2003601.
32. S. H. Shin, W. Lee, S. M. Kim, M. Lee, J. M. Koo, S. Y. Hwang, D. X. Oh and J. Park, *Chem. Eng. J.*, 2019, **371**, 452-460.
33. Z. Lei, Q. Wang, S. Sun, W. Zhu and P. Wu, *Adv. Mater.*, 2017, **29**, 1700321.
34. W. T. Dong, D. J. Yao and L. Yang, *Sensors*, 2020, **20**, 1641.
35. C. Yang, J. Dawulieti, K. B. Zhang, C. X. Cheng, Y. W. Zhao, H. Z. Hu, M. Li, M. Zhang, L. Chen, K. W. Leong and D. Shao, *Adv. Funct. Mater.*, 2022, **32**, 2111698.
36. R. Y. Li, Y. Y. Fan, L. L. Liu, H. N. Ma, D. Y. Gong, Z. H. Miao, H. Wang and Z. B. Zha, *Acs Nano*, 2022, **16**, 15026-15041.
37. Q. T. Chen, B. Yang, M. Y. Ding, Y. Pan, J. S. Qian, Z. Z. Zheng, B. Wu, J. B. Miao, R. Xia, Y. L. Tu and Y. Shi, *Eur. Polym. J.*, 2020, **140**, 110039.
38. Y. J. Li, S. Y. Shi, H. B. Cao and R. Q. Cao, *J. Membr. Sci.*, 2021, **625**, 119111.